An Improved State of Charge and State of Power Estimation Method Based on Genetic Particle Filter for Lithium-ion Batteries

Xingtao Liu [1,2], **Chaoyi Zheng** [1], **Ji Wu** [1,2,*], **Jinhao Meng** [3], **Daniel-Ioan Stroe** [4,*] and **Jiajia Chen** [1]

[1] Department of Vehicle Engineering, Hefei University of Technology, Hefei 230009, China; xingtao.liu@hfut.edu.cn (X.L.); yzzcy1994@163.com (C.Z.); chenjiajia@hfut.edu.cn (J.C.)
[2] Anhui Intelligent Vehicle Engineering Laboratory, Hefei 230009, China
[3] Department of Electrical Engineering, Sichuan University, Chengdu 610065, China; scmjh2008@163.com
[4] Department of Energy Technology, Aalborg University, 9220 Aalborg, Denmark
[*] Correspondence: wu.ji@hfut.edu.cn (J.W.); dis@et.aau.dk (D.-I.S.)

Abstract: In this paper, an improved method for estimating the state of charge (SOC) of lithium-ion batteries is proposed, which is developed from the particle filter (PF). An improved genetic particle filter (GPF), owing to the advantages of the PF and genetic algorithm, is proposed to overcome the disadvantage of the traditional particle filter: lacking the diversity of particles. Firstly, the relationship between SOC and open-circuit voltage (OCV) is identified on the low-current OCV test. Secondly, a first-order resistor and capacitance (RC) model is established, then, the least-squares algorithm is used to identify the model parameters via the incremental current test. Thirdly, GPF and the improved GPF (IGPF) are proposed to solve the problems of the PF. The method based on the IGPF is proposed to estimate the state of power (SOP). Finally, IGPF, GPF, and PF are employed to estimate the SOC on the federal urban driving schedule (FUDS). The results show that compared with traditional PF, the errors of the IGPF are 20% lower, and compared with GPF, the maximum error of the IGPF has declined 1.6% SOC. The SOC that is estimated by the IGPF is applied to estimate the SOP for battery, considering the restrictions from the peak SOC, the voltage, and the instruction manual. The result shows that the method based on the IGPF can successfully estimate SOP.

Keywords: lithium-ion battery; state estimation; state of charge; genetic particle filter; state of power

---

1. Introduction

Owing to the advantages of high-energy density, long cycle life, and no memory effect, lithium-ion batteries have drawn increasing attention from industry and academia [1]. As the primary power resource of electric vehicles (EVs), the lithium-ion battery has been studied for many years [2]. The state of charge (SOC) is one of the most significant parameters for the lithium-ion battery because the SOC of the cell represents the fuel gauge in an EV application. It is not only a crucial parameter for drivers but also an index in the battery management system (BMS) [3]. Without an accurate SOC knowledge, EVs would not meet the requirements for a safe and reliable operation, as the BMS would not manage to predict the driving range accurately nor to balance the battery cells [4]. On the other hand, the state of power (SOP) represents the available charging and discharging power for batteries. Estimating the SOP can help to confirm whether cells have sufficient energy to meet the demands of starting and acceleration for EVs and avoid overcharging or over-discharging [5]. More importantly, for EVs, the SOP can optimize the matching relationship between the battery and EVs, maximizing the energy recovery performance of EVs regenerative braking. At the same time, there is a close

relationship between SOC and SOP because the current and voltage are related to SOC. Therefore, it is necessary to obtain an accurate SOC before estimating the SOP.

To get an accurate SOC estimation, it is vital to reduce the influences of the system noise from the complex working environment of the EVs [6]. The noise, especially the nonlinear noise, would create huge errors when estimating the SOC. For this reason, there are various methods and improved methods to accurately estimate SOC at present. They can be divided into four categories: characteristic parameters-based methods, coulomb counting methods, data-driven methods, and model-based methods [7]. The first two types of methods are easy to implement; however, the first type of method can only be used in the laboratory environment, while the results from the second type of method cannot meet the requirement of modern EVs because of the effect of noise. The third type of method could achieve highly accurate results but needs lots of data to train before estimating the SOC. The steps of the fourth type of SOC estimating method consists of two parts. Firstly, battery models are built to imitate the dynamic characteristic of the battery. Secondly, algorithm filtering is applied to reduce the effect of noise. These methods can estimate SOC more accurately than the first two types of methods. Moreover, compared with the third type of methods, these methods do not need lots of data to train before estimating the battery SOC. Hence, these methods have attracted a lot of attention from academia. In this aspect, many researchers pay their attention to improve the algorithm's accuracy or simplify the calculation process of the algorithm. From the perspective of the algorithm, the Kalman filter and particle filter (PF) are studied a lot [6–16].

However, the traditional Kalman filter is only suitable for a linear system, but most noise in the environment of EVs is nonlinear. Therefore, it is necessary to improve the Kalman filter in order to get an accurate estimate of the SOC. In Reference [7], the cubature Kalman filter was proposed to overcome the effect of noise to estimate the SOC; then, a fuzzy controller was constructed to modify the gain coefficient of the filter. Compared with the cubature Kalman filter without the fuzzy controller, the new cubature Kalman filter had better accuracy. In Reference [8], Sun et al. improved the Kalman filter, combining the adaptive Kalman filter and the unscented Kalman filter to form the adaptive unscented Kalman filter, which can achieve accurate results and adaptively adjust the noise covariance. In Reference [9], SOC was estimated by the neural network and unscented Kalman filter. Firstly, SOC was estimated by a neural network, and the unscented Kalman filter was used to reduce the errors from the neural network. However, the calculation process was complicated.

Compared with the improved Kalman filter that applies Kalman gain to overcome the disadvantage of the Kalman filter, PF has been widely used to process the non-Gaussian random systems because of its ability to deal with nonlinear problems [10]. However, some particles would degenerate when the calculation is continuing, leading to a loss of diversity for the particles. Too much time will be spent on particles whose weight is low, causing the errors of the estimation if this problem is not solved. Therefore, how to increase the diversity of particles has become a hot research point. Xiong et al., in Reference [11], employed remaining available energy prediction and the SOC to test the uncertainties of temperature, then developed a double-scale PF to estimate the state and parameters of systems. For improving PF, a method using an extended Kalman filter to produce the importance of probability density function was proposed in Reference [12]. This method significantly improves the accuracy of PF. In Reference [13], Liu et al. proposed a dual-particle filter to obtain the SOC and the drift current based on a model keeping temperature and current as inputs to overcome the drifting noise and the effect of temperature. Combined with the PF and cubature Kalman filter, Xia et al., in Reference [14], proposed a new algorithm. The cubature Kalman filter generates the suggested density function for PF to obtain accurate estimations. Exploiting the two-dimensional model, an improved PF was developed in Reference [15] by independently sweeping in time and spatial coordinates. This improved PF can avoid repetitive solutions. In Reference [16], Shao et al. applied the recursive least square with forgetting factors to identify the parameters in the model. Then, the PF was employed to estimate the SOC in the experimental data from EVs in Beijing.

Estimating SOC accurately is the basis of reckoning SOP. The accurate SOP is beneficial for the vehicle by optimizing battery capacity and size [5]. SOP means how much power can batteries release or receive in a period. At present, there are two kinds of methods to estimate SOP: based on batteries experiment and based on models. The methods based on the batteries experiment are not widely used because sampling time is very short in the real situation. In this case, SOC and polarization voltage are usually neglected, which makes the result obtained from this method be enormously influenced [17]. So, researchers typically employ methods based on models to estimate SOP. In References [18,19], Wang et al. built a first-order equivalent circuit model to estimate the SOC and SOP, but the methods they used to estimate SOC were characteristic parameters-based methods and coulomb counting methods. These methods cannot reduce the effect of noise when calculating SOC in the real situation, affecting the accuracy of SOC a lot, which influences the accuracy of SOP directly. In Reference [20], the double Kalman filter was built to estimate SOP and identify the parameters of the model. This algorithm could estimate SOP accurately when the working situation was not very complicated. Waag et al. [21] considered the effect of resistance relying on current when estimating SOP, improving the accuracy. In Reference [22], a method based on the adapted Kalman filter with multiple restrictions was proposed to estimate the SOP. The estimations achieved from this method were exact. An improved method considering the effect of the state of health (SOH) to the SOP was presented in Reference [23]. The SOP was calculated with the SOC in the paper, which could reduce the errors that come from ignoring SOH.

Based on the research that has been listed, some algorithms which can accurately estimate SOC have the disadvantage of complicated steps, and some algorithms with simple steps cannot accurately estimate SOC. These algorithms not only decrease the working efficiency of BMS but also affect the estimation of SOP and the performance of EVs. In this paper, an improved algorithm, which can accurately estimate SOC with simple steps, is proposed. A genetic particle filter (GPF), combined with the features of a genetic algorithm, can overcome the disadvantage of the traditional PF by usefully increasing the diversity of particles. Moreover, in order to further improve the results, some changes are employed to the GPF for selecting the particles that own good weights. The improved GPF (IGPF) engages choosing, crossing, and variation instead of the traditional resample of PF, for increasing the diversity of particles. By comparing with the PF, the IGPF does not become very complicated while the results are improved considerably. The KF and the improved KF are only suitable in the environment of Gaussian noise. However, the IGPF is suitable in any noise environment. The KF and the improved KF must need the mean and variance of the process noise and measurement noise, which are difficult to obtain in a practical situation. But the IGPF only needs the variance of the measurement noise. These advantages increase the efficiency and practicality of the IGPF in the real situation. The SOP is divided into the discharging SOP and the charging SOP in this paper. The SOC estimated by the IGPF is used as parameters to calculate the SOP. Owing to the advantages of this new algorithm, SOP could be estimated successfully and efficiently. The outline of the paper is as follows: The introduction was presented in Section 1. Section 2 describes the battery model and identifies the parameters via the incremental current test. The relationship between the SOC and open-circuit voltage (OCV) is expressed through the low-current OCV test. The introduction about GPF and the IGPF and the detailed steps about the IGPF estimating SOC are shown in Section 3. The method of estimating SOP based on IGPF is shown in Section 4. Section 5 verifies the reliability and accuracy of IGPF for estimating the SOC and the methods based on IGPF for estimating SOP. The conclusions are given in Section 6.

2. Modeling and Parameters Identification

2.1. The Equivalent Circuit Model

In this paper, the test samples are 18,650 LiNiMnCoO2/Graphite lithium-ion cells, and the environment temperature is held at 25 °C. Their basic specifications are given in Table 1. The equivalent circuit models, which are composed of simple circuit elements, whose accuracy can be improved by

increasing the number of resistors and capacitances, have received much attention from academia [24]. This kind of model has been widely employed, built by a circuit network with a voltage source, capacitances, and resistances to simulate the external transient and characteristics of the batteries [25]. Compared with the other complex circuits, the first-order resistor and capacitance (RC) equivalent circuit model have the advantages of simple configuration, high accuracy, and easy parameterization. Based on these advantages, in this paper, a first-order RC equivalent circuit model is considered. The battery model is given in Figure 1. According to Figure 1, the discrete space equations of the first-order RC equivalent circuit model for estimating SOC can be expressed as follows [26–28]:

$$\begin{bmatrix} SOC_{k+1} \\ V_{p,k+1} \end{bmatrix} = \begin{bmatrix} 1 & 0 \\ 0 & e^{(-\Delta t/R_P C_P)} \end{bmatrix} * \begin{bmatrix} SOC_k \\ V_{p,k} \end{bmatrix} + \begin{bmatrix} -\eta \Delta t/Q \\ R_P(1 - e^{-\Delta t/R_P C_P}) \end{bmatrix} + w_k \tag{1}$$

$$V_k = OCV(SOC)_k - i_k * R_0 - V_{p,k} + v_k \tag{2}$$

where i_k is the current at time step k. In this paper, when the battery is charging, the current value is positive, and the current value is negative while the battery is discharging. Q is the nominal capacity of the cell. $V_{p,k}$ is the polarization voltage at time step k and η is the Coulomb efficiency. V_k is the load voltage at time step k. w_k is the noise of status, and v_k is the noise of measurement at time step k.

Table 1. Basic specifications of the battery.

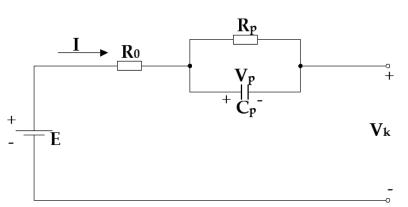| Type	Nominal Voltage	Nominal Capacity	Lower/Upper cut-off Voltage	Maximum Continuous Discharging Current
18,650	3.6 V	2.0 Ah	2.5 V/4.2 V	20 A (at 25 °C)

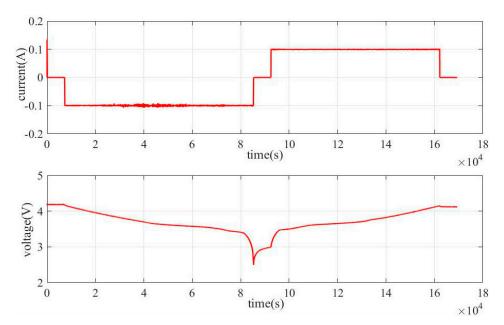**Figure 1.** Resistor and capacitance equivalent circuit model.

2.2. Parameters' Identification

After building the model, it is necessary to identify the parameters of the equation before estimating SOC and SOP. The parameters' identification is divided into two parts: status equation parameters identification and measurement equation parameters' identification. Firstly, the parameters on the measurement equation are determined on the low-current OCV test by fitting the curve of SOC and OCV. Secondly, the parameters on the status equation are identified via the incremental current test by the least-square algorithm.

2.2.1. OCV-SOC Mapping Test

In this paper, the low-current OCV test is applied to get the OCV-SOC curve. This test employs a small current (i.e., C/20) to charge and discharge the battery that makes the corresponding terminal voltage approximate to the OCV [29–32]. In this test, firstly, the cell is charged to the upper cut-off voltage by that constant current. Secondly, the cell is fully discharged until the voltage reaches the lower cut-off voltage. Then, the cell is charged again to the upper cut-off voltage. Finally, to reduce

the effects of hysteresis and resistance, the average voltage of the discharging and charging process is recorded as the OCV. The corresponding profile of current and voltage on the low-current OCV test is shown in Figure 2, and the curve of SOC and OCV is shown in Figure 3. The relationship between SOC and OCV is expressed by Equation (3). The errors between the real OCV and the measured OCV are given in Figure 4, and the values of a_i are shown in Table 2. The fitness of the curve is shown in Table 3.

$$OCV(SOC)_k = a_1 SOC_k{}^7 + a_2 SOC_k{}^6 + a_3 SOC_k{}^5 + a_4 SOC_k{}^4 + a_5 SOC_k{}^3 + a_6 SOC_k{}^2 + a_7 SOC_k + a_8 \quad (3)$$

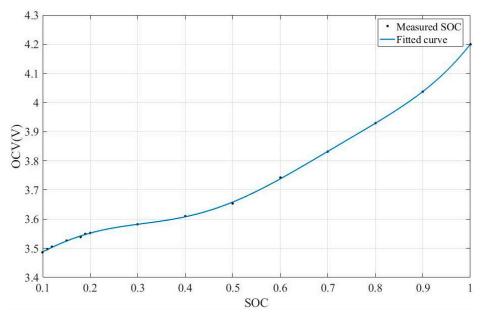**Figure 2.** Current and voltage of low-current open-circuit voltage test.
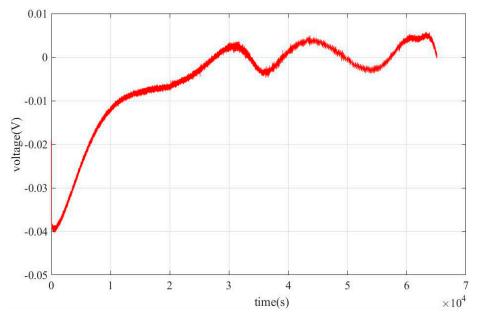

Figure 3. Curves at low-current OCV.

Figure 4. Errors between the real OCV and the calculated OCV.

Table 2. Data of the open-circuit voltage and State of Charge curve.

a_1	a_2	a_3	a_4	a_5	a_6	a_7	a_8
−57.54	227.1	−356.2	280.5	−114.4	22.62	−1.364	3.486

Table 3. The fitness of the curve.

SSE	R-Square	Adjusted	RMSE
$4.347 * 10^{-5}$	0.9998	0.9987	0.006593

The equation of the sum of squared errors (SSE) and root mean square error (RMSE) are expressed as follows:

$$SSE = \sum_{k=1}^{n} (f_k - y_k)^2 \tag{4}$$

$$RMSE = \sqrt{\sum_{k=1}^{n} (f_k - y_k)^2 / n} \tag{5}$$

where y_k is the real value at time step k, and f_k is the estimated value at time step k.

Owing to the feathers of the low-current OCV test, the relationship between the OCV and SOC can be obtained easily, which will be used in Equation (2) for the estimation of SOC. Moreover, from Table 3 and Figure 4, the errors between the real OCV and the calculated OCV are within 1% most of the time, and can meet the requirement of SOC estimation accuracy.

2.2.2. Model Parameters' Identification

The parameters of the model are identified via the incremental current test. The incremental current test is made up of numbers of SOC intervals and rest periods, after which the OCV and the results of SOC corresponding are obtained. In this test, firstly, the battery is charged to 100% SOC. Secondly, the cell is discharged at a constant current of 1/2C duration at every 10% SOC until the voltage drops to the lower cut-off voltage. Finally, the battery is charged by following the same routine but with a charging current until the voltage reaches the upper cut-off voltage. The profile of current and voltage in incremental current tests is shown in Figure 5. One set of model parameters is estimated

using the least-square algorithm on the incremental current test. The parameters' identification results are shown in Table 4.
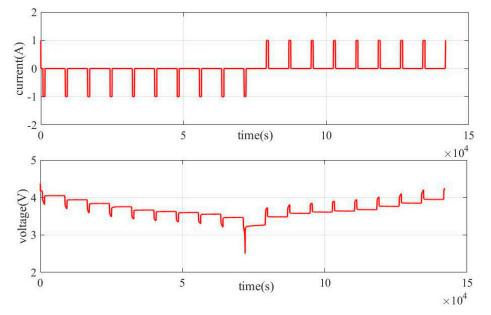

Figure 5. Current and voltage of the incremental current test.

Table 4. Model parameters and statistics.

Temperature	R_0	R_p	C_p	RMSE
25 °C	0.0710Ω	0.0342Ω	1135.2F	$5.98 * 10^{-4}$

Compared with the methods of online identification, the methods of offline identification have the advantages of less calculation, simple steps, and high efficiency. According to Table 4, on the incremental current test, the RMSE of the identification is within the allowable range, which means the results could be used further.

3. The IGPF Algorithm for SOC Estimation

3.1. The Steps of the IGPF

The genetic algorithm, which is from natural selection and genetic inheritance, can search the optimal solutions by simulating the process of natural evolution. Nowadays, this algorithm has been widely employed to search for the best solution from a sizeable multidimensional solution space [33]. The main steps of the genetic algorithm consist of choosing, which is used to select excellent offspring, and crossing, variation, which are employed to maintain the diversity of the population. The traditional resampling of the PF does not resolve the problem of lacking particle diversity and excellent particles, which could directly affect the accuracy of SOC estimating. Considering the disadvantages of PF, the genetic algorithm is suitable to displace the resampling of the traditional PF.

Usually, the sequence of the genetic algorithm is choosing, crossing, and variation. GPF's sequence of resampling is the same as the genetic algorithm. In the GPF, choosing is used to select particles with high weight, crossing and variation are employed to produce new particles, maintaining the diversity of the particles. The sequence of choosing, crossing, and variation are vital because the probability of getting excellent descendants is different. Compared to selecting particles with high weight before maintaining the diversity, choosing excellent particles after maintaining the diversity has a higher probability to obtain excellent particles. Hence, it is necessary to adjust the sequence of choosing, crossing, and variation. Compared with crossing, variation has a higher probability of getting particles

with poor quality, though it could still obtain particles with high weight and maintain the diversity of particles. Therefore, in this paper, the sequence of the GPF's resampling becomes crossing, variation, and choosing. Residual variation is employed to displace traditional variation for decreasing the negative effect of variation. The IGPF consists of the next steps.

1. Particles' initialization.

Setting the number of the particles as N and the number of the cycle as M, the initial value of x series is x_k^0. The particle sequence can be described as $\{x_k^0 | k = 1, 2 \ldots \ldots N\}$ based on x_k^0, and the particles have the same weight 1/N.

2. Status and measurement variables estimation.

x_k^i is the *i*th particle at time step k and y_k^i is the measurement variables of x_k^i. They are calculated by Equation (1), Equation (2), and Equation (3).

3. Calculating and updating the weight.

Equation (6) is used to calculate the weight of the particle at time step k. σ is the standard deviation of the measurement of noise.

$$q_k^i = (\frac{1}{\sqrt{2\pi}\sigma}) e^{\frac{(y_k - y_k^i)^2}{-2\sigma^2}} \tag{6}$$

Then, the weight of the particle is normalized by Equation (6):

$$q_k^i = \frac{q_k^i}{\sum q_k^i} \tag{7}$$

where q_k^i represents the weight of the *i*th particle at time step *k*.

4. Crossing.

A constant from zero to one is set as the crossing probability. At every cycle, a number subjected to the random distribution is produced. When the number is less than the crossing probability, the crossing is executed. Two particles, which are represented by x_k^i and x_k^j, are selected randomly. Equation (8) and Equation (9) are employed to cross the particles selected. In the following equations, *z* subjects the random distribution:

$$x_k^i = zx_k^i + (1-z)x_k^i \tag{8}$$

$$x_k^j = zx_k^j + (1-z)x_k^j \tag{9}$$

5. Variation.

A different constant is set as the variation probability. At every cycle, a number subjected to the random distribution is produced. If the number is less than the variation probability, the variation is executed. One particle, which is represented by x_k^b, is selected randomly. Equation (10) is used to execute the variation. In the following equation, *c* subjects the given Gaussian distribution:

$$x_k^b = x_k^b + c \tag{10}$$

$$c \sim N(0, y_k^i - x_k^i)$$

6. Choosing.

A number from zero to one is selected randomly, and the weight of particles is accumulated at every cycle. When the sum of the weight is more than the number that is selected, the process of accumulating is stopped. These accumulated particles are chosen to copy.

7.   Variables output.

The variables are calculated by Equation (11). The cycle is finished when the values of k are equal to the M. Otherwise, Step 2 will be carried out again.

$$x_k = \sum q_k^i x_k^i \tag{11}$$

3.2. Estimating SOC Based on the IGPF

To estimate SOC, the initial x is the value of initial SOC and x_k is the value of SOC at time step k. y_k is the value of the terminal voltage at time step k.

The workflow of estimating SOC by the IGPF is shown in Figure 6.

Figure 6. Process of the improved genetic particle filter method.

4. SOP Estimation Based on IGPF

4.1. The Considered Factors for Estimating SOP

In this paper, SOC, voltage, and the allowed current that comes from the instruction manual are considered when estimating SOP. It is necessary to take SOC into consideration. On the one hand, SOC has a close relationship with current and voltage, which are used to directly calculate SOP. On the other hand, the peak SOC could restrict the current, avoiding overcharging or over-discharging. However, the current limited by the peak SOC is too large to be used to directly calculate SOP. Therefore, it is necessary to take account of the influence of the voltage. The limits from the instruction manual are significant because the battery would be harmed, even explode when the actual current exceeds the allowed current. Thus, in this paper, the voltage, the SOC, and the limit from the instruction manual are considered to estimate SOP.

4.2. SOP Estimation by the Restricted Current

In this paper, the current is limited by three parts: the limit based on the peak of SOC, the limit based on voltage, and the allowed maximum charging current and discharging current that comes from the instruction manual of the battery. The values of SOC that are used to calculate the limited current are obtained by the IGPF.

4.2.1. Limit Based on the Peak SOC

In order to avoid overcharging and over-discharging, especially at the end of charging and discharging, the limit based on the peak of SOC is used. Otherwise, the life of the battery would be affected directly. When the value of SOC is near the peak SOC, the current must be limited to prevent overcharging or over-discharging from the aspect of capacity. The equations of current are expressed as follows:

$$i_{k,L}^{dis,s} = \frac{(SOC_k - SOC_{min}) * C_N}{TLh} \tag{12}$$

$$i_{k,L}^{cha,s} = \frac{(SOC_k - SOC_{max}) * C_N}{TLh} \tag{13}$$

where $i_{k,L}^{dis,s}$ is the discharging current restricted by the peak SOC at time step k. T represents the period of sampling and L is the number of sampling. $i_{k,L}^{cha,s}$ is the charging current restricted by SOC at time step k. SOC_{min} is the lowest of SOC and SOC_{max} is the highest of SOC. C_N is the nominal capacity of the battery and η is the Coulomb efficiency.

4.2.2. Limit Based on the Voltage

The limit that is only based on the peak SOC cannot meet the requirements. Not only is the current restricted by the peak SOC too large, but also the terminal voltage influenced by the polarization voltage reaches the protection condition before the effect of SOC. Therefore, restriction based on the voltage is employed.

According to Equation (2), the relationship between OCV and SOC is nonlinear. SOC_k is the function of the current. Thus, $OCV(SOC_k)$ cannot be used to directly calculate the peak current. Based on these reasons, the Taylor formula is employed. The new equation is expressed as follows:

$$OCV(SOC_{k+1}) = OCV(SOC_k) - \frac{i_k \eta \Delta t}{C_N} \frac{d(OCV)}{d(SOC)}|soc_k + R\left[SOC_k, \frac{i_k \eta \Delta t}{C_N}\right] \tag{14}$$

Because the R[.] is the remainder of the first-order expansion, and its variety is very tiny, therefore, in this paper, the value of R[.] is neglected. The equation of polarization voltage during the period of continuous time is given as follows:

$$Vp_{k,L} = V_{p,k}(e^{\frac{-\Delta t}{R_p C_p}})^L + i_k R_p (1 - e^{\frac{-\Delta t}{R_p C_p}}) \sum_{j=0}^{L-1} (e^{\frac{-\Delta t}{R_p C_p}})^{L-1-j} \tag{15}$$

where $Vp_{k,L}$ is the polarization voltage during the period of continuous time.

Based on Equation (14) and Equation (15), the current restricted by voltage is given as Equation (16) and Equation (17):

$$i_{k,L}^{dis,v} = \frac{OCV(SOC_k) - V_{p,k}(e^{\frac{-\Delta t}{R_p C_p}})^L - U_{min}}{\frac{\eta L \Delta t}{C_N} \frac{d(OCV)}{d(SOC)}|SOC_k + R_p (1 - e^{\frac{-\Delta t}{R_p C_p}}) \sum_{j=0}^{L-1} (e^{\frac{-\Delta t}{R_p C_p}})^{L-1-j} + R_0} \tag{16}$$

$$i_{k,L}^{cha,v} = \frac{OCV(SOC_k) - V_{p,k}(e^{\frac{-\Delta t}{R_p C_p}})^L - U_{max}}{\frac{\eta L \Delta t}{C_N} \frac{d(OCV)}{d(SOC)}|SOC_k + R_p (1 - e^{\frac{-\Delta t}{R_p C_p}}) \sum_{j=0}^{L-1} (e^{\frac{-\Delta t}{R_p C_p}})^{L-1-j} + R_0} \tag{17}$$

where U_{min} is the lower cut-off voltage and U_{max} is the upper cut-off voltage. $i_{k,L}^{dis,v}$ is the discharging current restricted based on voltage and $i_{k,L}^{cha,v}$ is the charging current restricted based on voltage.

4.2.3. Limit Based on the Instruction Manual of the Battery

According to the instruction manual of 18,650 LiNiMnCoO2/Graphite lithium-ion cells, the maximum continuous discharging current is 20 A, which is represented as i_{max}^{dis}, and the maximum continuous charging current is 4 A, which is described as i_{max}^{cha} [34].

4.2.4. SOP Estimation

The absolute minimum values are selected as the discharging current and the charging current when discharging and charging. Otherwise, the battery would be harmed. The equations of the current are given as follows:

$$i_{k,L}^{dis} = \min\left\{i_{k,L}^{dis,s}, i_{k,L}^{dis,v}, i_{max}^{dis}\right\} \tag{18}$$

$$i_{k,L}^{cha} = \max\left\{i_{k,L}^{cha,s}, i_{k,L}^{cha,v}, i_{max}^{cha}\right\} \tag{19}$$

where $i_{k,L}^{dis}$ is the discharging current during the period of continuous time and $i_{k,L}^{cha}$ is the charging current during the period of continuous time.

Equation (2) is the equation of voltage per second, which cannot be used to directly calculate the SOP. According to Equation (14) and Equation (15), the equation of terminal voltage during the period of continuous time can be calculated by Equation (20). However, the values of voltage and current that are calculated by the above Equations are changing all the time, causing the SOP to be changing at all times, which contradicts the definition of the SOP. The amount of calculations to estimate SOP whose values are almost unchanged at every period of continuous time is enormous. The values of the terminal voltage calculated by Equation (20) do not change too much at all times. Therefore, the terminal voltage at the time step $k + 1$ is employed to replace the voltage at the time step k to predict the voltage in the next period of continuous time. To reduce the amount of calculation and simplify the steps, the equations about discharging SOP and charging SOP could be calculated approximately by Equation (21) and Equation (22):

$$V_{k,L} = \text{OCV(SOC)}_k - i_k R_0 - \frac{i_k \eta T L}{C_N}\frac{d(\text{OCV})}{d(\text{SOC})}\bigg|_{\text{SOC}=\text{SOC}_k} - \left[\left(e^{\frac{-\Delta t}{R_p C_p}}\right)^L V_{p,k} + i_k R_p\left(1 - e^{\frac{-\Delta t}{R_p C_p}}\right)\sum_{j=0}^{L-1}\left(e^{\frac{-\Delta t}{R_p C_p}}\right)^{L-1-j}\right] \tag{20}$$

$$P_{k,L}^{dis} \approx i_{k,L}^{dis} * V_{k+1,L} \tag{21}$$

$$P_{k,L}^{cha} \approx i_{k,L}^{cha} * V_{k+1,L} \tag{22}$$

where $P_{k,L}^{dis}$ is the discharging SOP, and $P_{k,L}^{cha}$ is the charging SOP.

5. Results and Analysis

The values of crossing probability are usually from 0.6 to 0.8, and the values of variation probability are generally from 0.001 to 0.005. In these experiments, the probability of crossing is set as 0.7, and the probability of variation is set as 0.003. The number of particles is 200. The noise of the status equation and noise of the measurement equation are subjected to Gaussian distribution. The time interval is 10 s.

5.1. SOC Estimation Results

Estimation Results from IGPF, GPF, and PF

The federal urban driving schedule (FUDS), which is one of the most widely employed driving cycle tests in battery experiments, is performed to estimate the SOC of battery by the IGPF. The current of whole FUDS and the voltage of FUDS are shown in Figure 7. The results of the PF, GPF, and IGPF are given in Figure 8, and the errors between the real values and the estimation values are in Figure 9. In the actual situation, it is rare for batteries of EVs to release all-electric energy, 100% SOC, in one driving cycle. Therefore, in this paper, the range of SOC is set from 0.8 to 0.1.
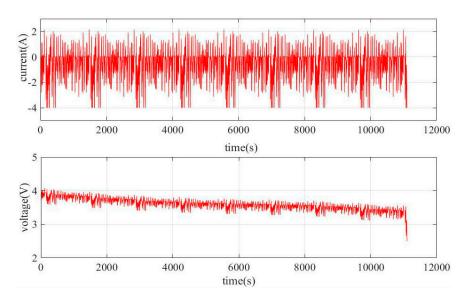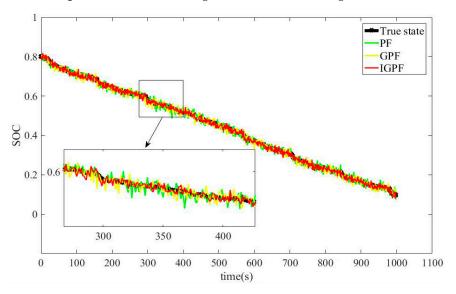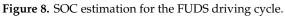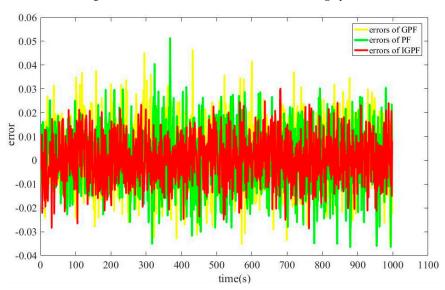
Figure 7. Current and voltage of federal urban driving schedule.

Figure 8. SOC estimation for the FUDS driving cycle.

Figure 9. Estimation errors for the FUDS driving cycle.

The equation of mean absolute error (MAE) is expressed as follows:

$$MAE = \frac{\sum\limits_{k=1}^{n} |f_k - y_k|}{n} \tag{23}$$

where y_k is the real value at time step k, and f_k is the estimated value at time step k.

The RMAE, MAE, and the maximum error of PF and IGPF are shown in Table 5. The computational time of these algorithms is in Table 6.

Table 5. Avenue errors and the maximum errors of three algorithms.

Algorithm	RMSE	MAE	The Maximum Error
PF	0.01254921	0.00930901	0.051
IGPF	0.00997832	0.00810877	0.030
GPF	0.01338364	0.01058916	0.046

Table 6. Comparison of the computational time.

Algorithm	The Computational Time
PF	4 s
IGPF	6 s
GPF	10 s

As can be seen from the figures and the table above, the accuracy of the IGPF is better than the traditional PF and the GPF. The accuracy of the IGPF is 20% higher than the PF, and 15% higher than the GPF. At the same time, the maximum error of the IGPF declines 2% SOC more than the PF and 1.6% SOC more than the GPF. Owing to the advantages of crossing and variation, the diversity of particles has increased compared with the traditional PF. The probability of particles with high quantity increases, resulting from the application of residual variation and the sequence change of the choosing, crossing, and variation, which makes the results more accurate than the GPF.

According to Table 6, the computational time of the PF is shorter than the IGPF and the GPF; however, compared with the PF, the time of the IGPF is just 2 s longer. This means the calculation of the IGPF does not increase too much. Therefore, it is very suitable to be employed in a real situation. Since the calculation of crossing and variation become huge after choosing, the computational time of the GPF is longer than the IGPF. Thus, not only from the aspect of accuracy but also from the length of computational time, the IGPF is more effective and practical than the GPF.

5.2. SOP Estimation Results

In this paper, SOP is defined as the power that the battery can release or receive during the period of continuous time when discharging or charging without harming the battery. Thus, it is meaningless to estimate SOP per second. The sampling time is set as 10 seconds in this paper because the range of SOC above is from 0.8 to 0.1 approximately in order to reflect the real situation in this paper. Therefore, the values of SOC_{min} is set as 0.1, and the value of SOC_{max} is set as 0.8. The SOC, estimated by the IGPF, comes from Section 4. The estimated discharging SOP and charging SOP are presented in Figure 10. The SOP which is calculated by different limitations is plotted in Figure 11. The discharging SOP is defined as positive numbers, while the charging SOP is defined as negative numbers in this paper.
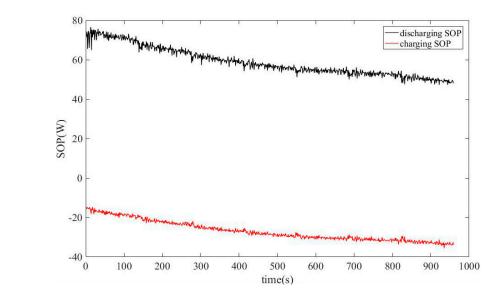
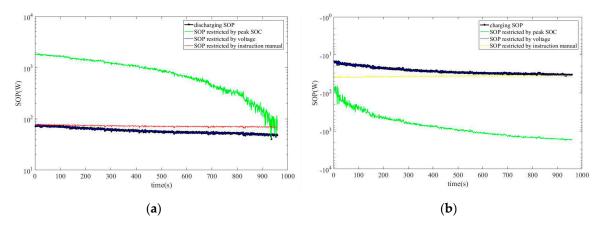**Figure 10.** SOP and charging SOP on the FUDS.

(**a**)   (**b**)

Figure 11. (**a**) SOP and (**b**) charging SOP with different limitations on the FUDS.

From these curves, the changing trend of SOP is roughly similar to the voltage, which reflects the accuracy of the results. At the beginning of FUDS, the values of the discharging SOP are tremendous results from the high SOC. On the contrary, the values of the charging SOP are lower than the discharging SOP. With the continuing of FUDS, the battery releases more energy than it receives, declining the SOC and the terminal voltage, which leads the values of discharging SOP to gradually become small. The values of charging SOP become more significant than before, because of the loss of numerous electricity.

From these figures, the SOP restricted by the peak SOC does not affect the charging and discharging SOP too much because the values of current which are only limited by the peak SOC are larger than the current that is allowed by the instruction manual most of the time.

For the discharging SOP, in the beginning, the SOP restricted by voltage dominates the values because the SOP restricted by peak SOC is too large. With the continuing of discharging, the values limited by voltage reduce because the voltage becomes small. In the end, the change of SOC affects the discharging SOP more than the effects that come from the change of terminal voltage at some moments, causing the limitation restricted by the peak SOC to dominate the discharging SOP.

The charging SOP restricted by voltage dominates the charging SOP due to the fact that the value of current restricted based on peak SOC is larger than the allowed values in the beginning. Gradually, the values of the charging SOP become more significant than before. In the end, the values of the charging SOP are near the allowed values, which correspond to the real situation.

6. Conclusions

In order to estimate SOC accurately and simply, a first-order equivalent circuit model was built to imitate the dynamic characteristics of the battery. The relationship between SOC and OCV was identified by the data of the low-current OCV test, and the parameters of the model were identified via the data of the incremental current test. Based on the circuit model and the parameters, the IGPF is proposed to estimate the SOC. As the results of the experiment showed, compared with the GPF and PF, the IGPF has higher accuracy because crossing and residual variation could increase the diversity of particles significantly with simple steps and less calculation, and choosing could obtain particles with high weights, which overcome the drawbacks of the PF. Therefore, the IGPF has more practicality and efficiency than other algorithms with complex and huge calculations.

In this paper, the SOP is estimated based on the estimated SOC. The limitations which take the influences of the SOC, voltage, and instruction manual into consideration are employed to estimate the discharging SOP and charging SOP. The values of discharging SOP decrease gradually from a tremendous value. The values of charging SOP increase gradually to a stable value. These changing trends correspond with the actual situation, reflecting the reliability of the estimations.

Author Contributions: Methodology, C.Z.; Writing—original draft, C.Z.; Writing—review & editing, X.L., J.W., J.M., D.-I.S. and J.C. All authors have read and agreed to the published version of the manuscript.

Conflicts of Interest: The authors declare no conflict of interest.

References

1. Meng, J.H.; Luo, G.Z.; Ricco, M. Overview of Lithium-ion Battery Modeling Methods for State-of-Charge Estimation in Electrical Vehicles. *Appl. Sci.* **2018**, *8*, 659. [CrossRef]
2. Liu, X.T.; He, Y.; Zheng, X.X. A new State-Of charge estimation method for electric vehicle lithium-ion batteries on multiple input parameter fitting model. *Energy Res.* **2017**, *41*, 1265–1276. [CrossRef]
3. Meng, J.H.; Ricco, M.; Acharya, A. Low-Complexity online estimation for LiFePO4 battery state of charge in electric vehicles. *J. Power Sources* **2018**, *395*, 280–288. [CrossRef]
4. Marongiu, A.; Roscher, M.; Sauer, D.U. Influence of the vehicle-to grid strategy on the aging behavior of lithium battery electric vehicles. *Appl. Energy* **2015**, *137*, 899–912. [CrossRef]
5. Liu, X.T.; He, Y.; Zhang, J.F. A Method for State-of-Power Estimation of Li-ion Battery Considering Battery Surface Temperature. *Energy Technol.* **2018**, *10*, 1002–1010.
6. Xia, B.Z.; Guo, S.K.; Wang, W. A State of Charge Estimation Method Based on Adaptive Extended Kalman-Particle Filtering for Lithium-ion Battery. *Energies* **2018**, *11*, 2755. [CrossRef]
7. Peng, J.K.; Luo, J.Y.; He, H.W. An improved state of charge estimation method based on cubature Kalman filter for lithium-ion batteries. *Appl. Energy* **2019**, *253*, 113520. [CrossRef]
8. Sun, F.; Hu, X.; Zou, Y.; Li, S. Adaptive unscented Kalman filtering for state of charge estimation of a lithium-ion battery for electric vehicles. *Energy* **2014**, *134*, 3531–3540. [CrossRef]
9. He, W.; Nicholas, W.; Chen, C.C. State of Charge estimation for Li-ion batteries using neural network modeling and unscented Kalman filter-based error cancellation. *Electr. Power Energy Syst.* **2014**, *62*, 783–791. [CrossRef]
10. Li, B.; Peng, K.; Li, G.D. State-of Charge estimation for lithium-ion battery using the Gauss-Hermite particle filter technology. *J. Renew. Suitable Energy* **2018**, *10*, 041015.
11. Xiong, R.; Zhang, Y.Z.; He, H.W. A Double-Scale, Particle-Filtering, Energy State Prediction Algorithm for Lithium-ion Batteries. *IEEE Trans. Ind. Electron.* **2018**, *65*, 1526–1538. [CrossRef]

12. Aslan, S. Comparison of the hemodynamic filtering methods and particle filter with extended Kalman filter approximated proposal function as an efficient hemodynamic state estimation method. *Biomed. Signal Process.* **2016**, *25*, 99–107. [CrossRef]

13. Liu, X.T.; Chen, Z.H.; Zhang, C.B.; Wu, J. A novel temperature-compensated model for power Li-ion batteries with dual-particle-filter state of charge estimation. *Appl. Energy* **2014**, *123*, 263–272. [CrossRef]

14. Xia, B.Z.; Sun, Z.; Zhang, R.F. A cubature particle filter algorithm to estimate the state of charge of Lithium-ion batteries based on a second-order equivalent circuit model. *Energies* **2017**, *10*, 457. [CrossRef]

15. Tulsyan, A.; Tsai, Y.; Gopaluni, R.B. State-of-charge estimation in lithium-ion batteries: A particle filter approach. *J. Power Sources* **2016**, *331*, 208–233. [CrossRef]

16. Shao, S.; Bi, J.; Yang, F. On-line estimation of state-of-charge of Li-ion batteries in electric vehicle using the resampling particle filter. *Transp. Res. Part D Transp. Environ.* **2013**, *32*, 207–217. [CrossRef]

17. Wik, T.; Fridholm, B.; Kuusisto, H. Implementation and Robustness of an Analytically Based Battery State of Power. *J. Power Sources* **2015**, *287*, 448–457. [CrossRef]

18. Wang, S.; Verbrugge, M.; Wang, J.S. Power Prediction from a Battery State Estimator that Incorporates Diffusion Resistance. *J. Power Sources* **2012**, *214*, 399–406. [CrossRef]

19. Wang, S.; Verbrugge, M.; Wang, J.S. Multi-parameter Battery State Estimator Based on the Adaptive and Direct Solution of the Governing Differential Equations. *J. Power Sources* **2011**, *196*, 8735–8741. [CrossRef]

20. Pei, L.; Zhu, C.; Wang, T. Online peak power prediction based on a parameter and state estimator for lithium-ion batteries in electric vehicles. *Energy* **2014**, *66*, 766–778. [CrossRef]

21. Waag, W.; Fleischer, C.; Sauer, D.U. Adaptive on-line prediction of the available power of lithium-ion batteries. *J. Power Sources* **2013**, *242*, 548–559. [CrossRef]

22. Xiong, R.; Sun, F.; He, H. A data-driven Adaptive State of Charge and Power Capability Joint Estimator of Lithium-ion Polymer Battery used in Electric Vehicles. *Energy* **2013**, *63*, 295–308. [CrossRef]

23. Sun, F.; Xiong, R.; He, H. Estimation of State-of-charge and State-of-power Capability of Lithium-ion Battery Considering varying Health Conditions. *J. Power Sources* **2014**, *259*, 166–176. [CrossRef]

24. Rahimi, E.H.; Chow, M.Y. Adaptive parameter identification and State-of-Charge estimation of lithium-ion batteries. In Proceedings of the IECON 2012—38th Annual Conference on IEEE Industrial Electronics Society, Montreal, QC, Canada, 25–28 October 2012.

25. Li, J.H.; Gao, F.J.; Yan, G.G.; Zhang, T.Y. Modeling and SOC estimation of lithium iron phosphate battery considering capacity loss. *Prot. Control Mod. Power Syst.* **2019**, *3*, 5. [CrossRef]

26. Kim, T.H.; Moon, K.R. Variable-structured interacting multiple model algorithm for the ballistic coefficient estimation of a re-entry ballistic target. *Int. J. Autom. Control* **2013**, *11*, 1204–1213. [CrossRef]

27. Zheng, F.; Jiang, J.; Sun, B. Temperature dependent power capability estimation of lithium-ion batteries for hybrid electric vehicles. *Energy* **2016**, *113*, 64–75. [CrossRef]

28. Dong, S.; Wang, W.; Sun, B. Software development method of battery SOC estimation based on target link. *Electr. Power Constr.* **2015**, *36*, 181–186.

29. Xing, Y.J.; He, W.; Pecht, M.; Tsui, K.L. State of charge estimation of lithium-ion batteries using the open-circuit voltage at various ambient temperatures. *Apply Energy* **2014**, *113*, 106–115. [CrossRef]

30. He, W.; Williard, N.; Chen, C.C.; Pecht, M. State of charge estimation for electric vehicle batteries using unscented kalman filtering. *Microelectron. Reliab.* **2013**, *53*, 840–847. [CrossRef]

31. Plett, G.L. Extended Kalman filtering for battery management systems of LiPB-based HEV battery packs—Part 2. Modeling and identification. *J. Power Sources* **2004**, *134*, 262–276. [CrossRef]

32. Dai, H.F.; Wei, X.Z.; Sun, Z.C.; Wang, J.Y.; Gu, W.J. Online cell SOC estimation of Li-ionbattery packs using a dual time-scale Kalman filtering for EV applications. *Apply Energy* **2012**, *95*, 227–237. [CrossRef]

33. Chen, L.; Wang, Z.Z.; Lü, Z.Q. A Novel State-of-Charge Estimation Method of Lithium-ion Batteries Combining the Grey Model and Genetic Algorithms. *IEEE Trans. Power Electron.* **2018**, *30*, 8797–8870. [CrossRef]

34. Samsung SDI Co., Ltd. *111219_INR18650-20R Cell SPEC Ver 1 0*; Samsung SDI Co., Ltd.: Kyeonggi City, Korea, 2011.